LIMIT STATE ANALYSIS OF ASYMMETRICAL MICROSTRUCTURES BASED ON YIELD DESIGN COMPUTATIONAL HOMOGENIZATION APPROACH

Phuc L. H. Ho[1,2] ⓘ**, Canh V. Le**[1,2,*] ⓘ**, Phuong H. Nguyen**[1,2] ⓘ**, Chanh T. Ngo**[3]

[1]*School of Civil Engineering and Management, International University, VNU-HCMC, Ho Chi Minh City, Vietnam*
[2]*Vietnam National University, Ho Chi Minh City, Vietnam*
[3]*Mien Tay Construction University, Vinh Long, Vietnam*
*E-mail: lvcanh@hcmiu.edu.vn

Abstract. This paper presents a novel formulation for the computational homogenization analysis of materials at the limit state. The polynomial interpolations are employed to impose the periodic boundary conditions for the fluctuating term of the displacement field when using arbitrary finite element meshes. Second-order cone programming provides an efficient solution to solve the resulting optimization problems, and accurate load multipliers can be obtained with the minimum computational cost. Several asymmetrical material models are investigated to perform the efficiency of the proposed method. The collapse mechanisms of the representative volume elements are also presented.

Keywords: homogenization analysis, periodic, polynomial interpolation, limit analysis, SOCP.

1. INTRODUCTION

The computational homogenization analysis is an effective method for estimating the effective properties of heterogeneous materials, particularly for non-linear structural behaviors [1–4]. The basic idea of such an approach is to couple two computational models, including a macro-scale and a micro-scale. The macroscopic properties are determined by solving an auxiliary boundary value problem defined on a representative volume element (RVE).

In computational homogenization analysis, the accuracy in predicting macroscopic behaviors is strongly affected by how the RVE boundary conditions are treated. Among classical boundary conditions satisfying macro-homogeneity: Dirichlet, Neumann, and Periodic, many studies demonstrated that the periodic boundary condition is the most efficient [5, 6]. The periodicity constraints require the conformity of nodal distribution

on opposite boundaries of RVE, meaning that nodes on the positive and negative sides must match in pairs. Generally, it is difficult to guarantee that requirement, particularly for complicated RVE models. In the last two decades, several efforts to maintain the periodicity of non-periodic meshes have been proposed. Tyrus et al. [7] introduced an approach utilizing the cubic and linear interpolants to model the displacement fields at the matrix and fiber edges on the boundary, respectively. Yuan and Fish [8] used an interesting approach, the so-called master-slave, to enforce the periodic boundary condition. A polynomial interpolation method involving Lagrange and Cubic spline formulation was suggested in [9]. More recently, Wang et al. [10] presented a strategy based on the radial point interpolation method imposing periodic boundary conditions over non-periodic meshes.

This work aims to predict the ultimate effective properties of heterogeneous materials using the kinematic yield design homogenization approach developed in [11–14]. The fluctuating part of the displacement field is approximated using the finite element method. The polynomial interpolating technique reported in [9] is employed to implement the periodic boundary conditions over non-symmetrical finite element meshes. The formulation of plastic dissipation power is transformed into a sum of Euclidean norms, allowing the primal-dual interior point algorithm to solve the resulting optimization problems.

2. KINEMATIC LIMIT ANALYSIS BASED ON COMPUTATIONAL HOMOGENIZATION

In homogenization analysis, the effective properties of a heterogeneous material can be estimated by solving the problem formulated at the microscopic level. Any material point x of a body is assigned as a representative volume element (RVE) with appropriate boundary conditions. Consider a rigid-perfectly plastic RVE with the boundary Ω, kinematic boundary Γ_u, and subjected to macroscopic pressure $\lambda\Sigma$. The microscopic fields are decomposed into two parts, including an averaged term and a periodic term, as follows

$$u = E.x + \tilde{u}, \tag{1}$$

$$\varepsilon = E + \tilde{\varepsilon}, \tag{2}$$

$$\sigma = \Sigma + \tilde{\sigma}, \tag{3}$$

where $\tilde{u}, \tilde{\varepsilon}, \tilde{\sigma}$ denote the fluctuating parts of the displacement field u, strain ε, and stress σ at the microscopic scale. The overall strain and stress are linked to microscopic quantities via the average relation

$$E \equiv \langle \varepsilon \rangle = \frac{1}{\Omega} \int_{\Omega} \varepsilon d\Omega, \tag{4}$$

$$\Sigma \equiv \langle \sigma \rangle = \frac{1}{\Omega} \int_{\Omega} \sigma d\Omega. \tag{5}$$

In the framework of yield design homogenization approach, the kinematic theorem can be expressed as

$$\lambda^+ \Sigma^T E \leq \int_\Omega D(\varepsilon)\, d\Omega, \tag{6}$$

where the plastic dissipation power can be calculated by

$$D(\varepsilon) = \int_\Omega \sqrt{\varepsilon^T \Theta \varepsilon}\, d\Omega = \int_\Omega \sqrt{(E + \tilde{\varepsilon})^T \Theta (E + \tilde{\varepsilon})}\, d\Omega. \tag{7}$$

Using the von Mises yield criterion, Θ can be determined as follows

$$\Theta = \sigma_p \begin{bmatrix} 1 & -1/2 & 0 \\ -1/2 & 1 & 0 \\ 0 & 0 & 3 \end{bmatrix}^{-1}, \tag{8}$$

where σ_p is the plastic stress of material.

The explicit formulation of the kinematic yield design homogenization approach can be now expressed as follows

$$\lambda^+ = \min \int_\Omega \sqrt{(E + \tilde{\varepsilon})^T \Theta (E + \tilde{\varepsilon})}\, d\Omega, \tag{9a}$$

$$\text{s.t.} \begin{cases} \Sigma^T E = 1, & \text{in } \Omega \\ \tilde{u}, & \text{periodic on } \Gamma_u \end{cases} \tag{9b}$$

3. IMPOSING PERIODIC BOUNDARY CONDITION FOR RVE WITH NON-PERIODIC MESHES

Enforcing the periodic boundary condition (PBC) plays a crucial role in computational homogenization analysis. It guarantees the continuity between neighboring RVEs and ensures the periodicity of mechanical fields. The boundary of RVE is divided into associated parts on opposite edges, then the periodic condition for every pair of points (x^+, x^-) on the positive and negative boundary (Γ^+, Γ^-) is imposed as follows

$$\tilde{u}(x^+) = \tilde{u}(x^-). \tag{10}$$

In numerical implementation, the condition in Eq. (10) requires an adequate mirrored discretization on opposite RVE boundaries. That is not always satisfied for arbitrary meshes, however. The topological difference between the opposite faces may make this enforcement impossible. This study suggests a treatment for this difficulty. The idea here is that a set of artificial nodes, which are periodic in pairs, are created on the edges of the RVE, and the displacement field on each edge is interpolated using the Lagrange formulation or the cubic spline formulation, as shown in Fig. 1. This allows the PBC for general mesh design to be imposed efficiently.

(a) Periodic boundary condition   (b) Polynomial interpolation
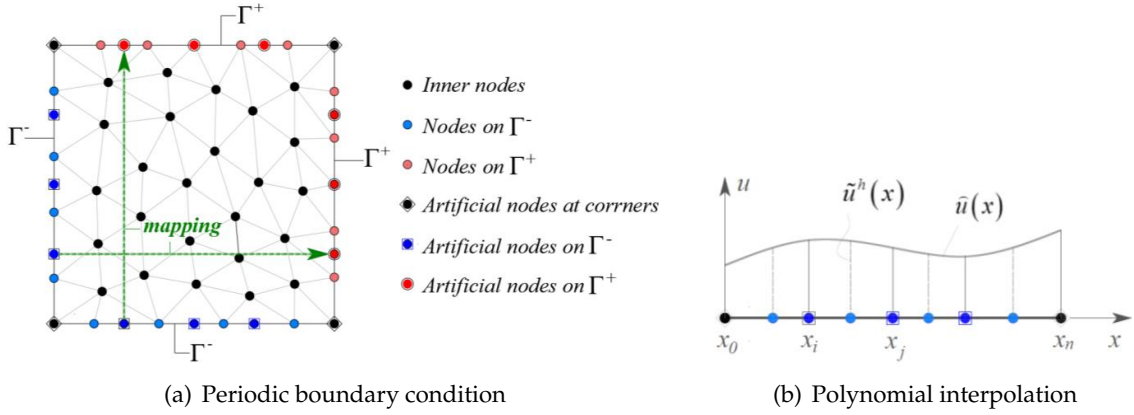
Fig. 1. Enforcement of periodic boundary condition using polynomial interpolation

3.1. Lagrange formulation

The displacement of nodes on an edge can be approximated using the polynomial $\mathbf{S}$ of order s as follows

$$\tilde{u}^h(x) = \mathbf{S}(x) = \sum_{i=0}^{s} L_i(x)\,\widehat{u}_i, \tag{11}$$

where $\widehat{u}_i$ denote the displacement of sampling point x_i, $L_i(x)$ is the Lagrange polynomial which is given by

$$L_i(x) = \prod_{j=0,j\neq i}^{s} \frac{x - x_j}{x_i - x_j}. \tag{12}$$

Noting that the function $L_i(x)$ satisfy Kronecker delta property and the norm

$$\sum_{i=0}^{s} L_i(x) = 1. \tag{13}$$

3.2. Cubic spline formulation

An edge is divided into s segments for this formulation, resulting in $s+1$ sampling points. In each segment, the displacement field can be interpolated using the Hermite polynomial as follows

$$\tilde{u}^h(x) = H_1(\zeta)\,\widehat{u}_i + H_2(\zeta)\,\widehat{\theta}_i + H_3(\zeta)\,\widehat{u}_j + H_4(\zeta)\,\widehat{\theta}_j, \tag{14}$$

where $\widehat{u}_i, \widehat{u}_j$ are displacements, and $\widehat{\theta}_i, \widehat{\theta}_j$ are slopes of the sampling points at two ends of the segment, the functions $H_1(\zeta), H_2(\zeta), H_3(\zeta), H_4(\zeta)$ are given by

$$H_1(\zeta) = 1 - 3\zeta^2 + 2\zeta^3, \tag{15a}$$

$$H_2(\zeta) = \delta_s \left(\zeta - 2\zeta^2 + \zeta^3\right), \tag{15b}$$

$$H_3(\zeta) = 3\zeta^2 - 2\zeta^3, \tag{15c}$$

$$H_4(\zeta) = \delta_s \left(-\zeta^2 + \zeta^3\right), \tag{15d}$$

where $\varsigma(x) = \dfrac{x - x_i}{\delta_s}$, $\delta_s = x_j - x_i$ is the segment length.

It is worth noting that the artificial nodes may coincide with the natural boundary nodes. The number of additional variables per each artificial node is 2 when using Lagrange interpolation, whereas those variables using cubic spline interpolation are 4. The shape function of Lagrange formulation and cubic spline formulation with the third-degree polynomial are illustrated in Fig. 2.

(a) Lagrange interpolating polynomial   (b) Cubic spline polynomial
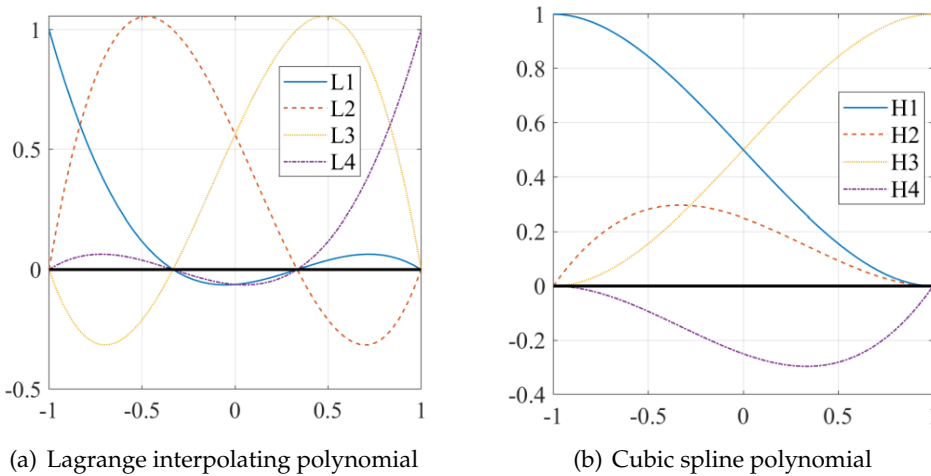
Fig. 2. The shape function of Lagrange and cubic spline formulations (3rd degree polynomial)

4. NUMERICAL IMPLEMENTATION

In the framework of finite element implementation, the problem domain is discretized to N_e triangle elements $\Omega^1 \cup \Omega^2 \cup \dots \Omega^{N_e} \approx \Omega$ such that $\Omega^1 \cap \Omega^2 \cap \dots \Omega^{N_e} = \emptyset$. The displacement field is approximated as

$$u^h(x) = \sum_{i=1}^{N} N_{1i}(x)\tilde{u}_i + \sum_{j=1}^{M} N_{2j}(x)\widehat{u}_j = \begin{bmatrix} N_1 & G_1 \\ G_2 & N_2 \end{bmatrix} \left\{ \begin{array}{c} \tilde{d} \\ \widehat{d} \end{array} \right\} = Nd, \tag{16}$$

where N_1 and N_2 are the usual linear shape function, G_1 and G_2 are the zero matrices associated to the additive periodic variables, the fluctuation displacement vector $\tilde{d}$ and the independent displacement vector $\widehat{d}$ are given by

$$\tilde{d}^T = \left[\tilde{u}_{1x}, \tilde{u}_{1y}, \tilde{u}_{2x}, \tilde{u}_{2y}, \ldots, \tilde{u}_{Nx}, \tilde{u}_{Ny} \right],$$ (17a)

$$\widehat{d}^T = \left[\widehat{u}_{1x}, \widehat{u}_{1y}, \widehat{u}_{2x}, \widehat{u}_{2y}, \ldots, \widehat{u}_{Mx}, \widehat{u}_{My} \right], \text{ for Lagrange interpolation}$$ (17b)

$$\widehat{d}^T = \left[\widehat{u}_{1x}, \widehat{\theta}_{1x}, \widehat{u}_{1y}, \widehat{\theta}_{1x}, \widehat{u}_{2x}, \widehat{\theta}_{2x}, \widehat{u}_{2y}, \widehat{\theta}_{2x}, \ldots, \widehat{u}_{Mx}, \widehat{\theta}_{Mx}, \widehat{u}_{My}, \widehat{\theta}_{Mx} \right], \text{ for cubic spline interpolation}$$ (17c)

where N is number of discretized nodes, and M is number of periodic artificial nodes.

The strain field can be calculated by

$$\tilde{\varepsilon}^h (x) = \left[\begin{array}{cc} B_1 & G_1 \\ G_2 & G_3 \end{array} \right] \left\{ \begin{array}{c} \tilde{d} \\ \widehat{d} \end{array} \right\} = Bd,$$ (18)

where B_1 denotes strain-displacement matrix consisting of the shape function derivatives, G_1, G_2 and G_3 are the null matrices.

The plastic dissipation power of RVE can be rewritten as

$$D(\varepsilon) = \sum_{i=1}^{N_g} \xi_i \sigma_p \sqrt{(E + Bd)^T \, \Theta \, (E + Bd)},$$ (19)

where N_g and ξ are the number of Gaussian points and their integral weights over Ω.

Introducing the additional variable vector $\chi = [\chi_1, \chi_2, \chi_3]^T$ associated with every Gaussian point in Ω such that

$$\chi = J(E + B_i d),$$ (20)

where J is the Cholesky factor of Θ, the plastic dissipation power can be computed in the form containing a sum of norms as

$$D(\varepsilon) = \sum_{i=1}^{N_g} \xi_i \sigma_p \|\chi_i\|,$$ (21)

where $\|.\|$ denotes the Euclidean norm.

The periodic condition for every pair of artificial nodes (x^+, x^-) can be expressed as

$$\widehat{u}(x^+) - \widehat{u}(x^-) = 0$$ (22)

The displacements of natural nodes on the boundary $\tilde{u}_{BC}^h$ are interpolated pass through those of periodic artificial nodes as

$$\tilde{u}_{BC}^h (x) = \sum_{j=1}^{M} \widehat{N}_j (x) \widehat{u}_j,$$ (23)

which can be then expressed in the matrix form as

$$N_1^* \tilde{d} - \widehat{N} \widehat{d} = 0,$$ (24)

where N_1^* is the extraction of N_1 for the boundary nodes, $\widehat{N}$ is the interpolating shape function obtained using the Lagrange or cubic spline formulations.

Assembling to the global system, Eqs. (22) and (24) can be combined and rewritten as

$$Cd = 0. \tag{25}$$

By introducing the auxiliary variables $t = \left[t_1, t_2, \ldots, t_{N_g}\right]$, the kinematic yield design homogenization for a periodic structure can be cast in the form of a standard conic programming problem as

$$\lambda^+ = \min \sum_{i=1}^{N_g} \xi_i \Omega_i t_i, \tag{26a}$$

$$\text{s.t.} \begin{cases} \Sigma^T E = 1 \\ Cd = 0 \\ \|\chi_i\| \leq t_i, \quad i = 1, 2, \ldots, N_g \end{cases} \tag{26b}$$

The numerical implementation of the optimization problem (26) is performed in MATLAB and efficiently solved using the primal-dual interior point algorithm integrated into the MOSEK solver. It is worth noting that the solutions obtained from the problem (26) are not guaranteed the strict upper bound property. The reasons are that the constraints are only satisfied at the Gaussian points, and the periodic boundary conditions are indirectly enforced by interpolating the fluctuation displacements of nodes on the boundary passing through those of the artificial periodic points.

5. NUMERICAL RESULTS

Several problems are investigated in this section to perform the computational efficiency of the proposed method. The square RVE of dimension $L \times L = 1 \times 1$ (mm) are used, and the materials are assumed to be isotropic and obey the von Mises yield criterion for all examples.

5.1. RVE with a circular perforate at the center

This example considers a material model with a circular perforate at the center and subjected to an orthotropic macroscopic loading $(\Sigma_{11}, \Sigma_{22})$, as shown in Fig. 3(a). The angle between the macroscopic pressure Σ_{11} and the x-axis is θ. The matrix material is Aluminum (Al) with yield stress $\sigma_p = 137$ MPa. This benchmark problem has been investigated in the works of Li et al. [12] and Le et al. [13] using finite element method, and Ho et al. [14] using the iRBF mesh-free method.

In this study, three different boundary enforcement strategies are employed to examine the performance of the proposed method. These are the standard periodic boundary scheme, Lagrange interpolating formulation, and cubic spline interpolating formulation. Figs. 3(b) and 3(c) illustrate the symmetrical and asymmetrical meshes for such techniques, where (n_L, n_R, n_B, n_T) are the number of nodes on the left, right, bottom, and top edges of the RVE, respectively. For the asymmetrical boundary, each RVE edge is divided

(a) Geometry, boundary, and loading

(b) Symmetrical mesh $n_L = n_R = n_B = n_T = 23$

(c) Asymmetrical mesh $[n_L, n_R, n_B, n_T] = [23, 27, 21, 35]$
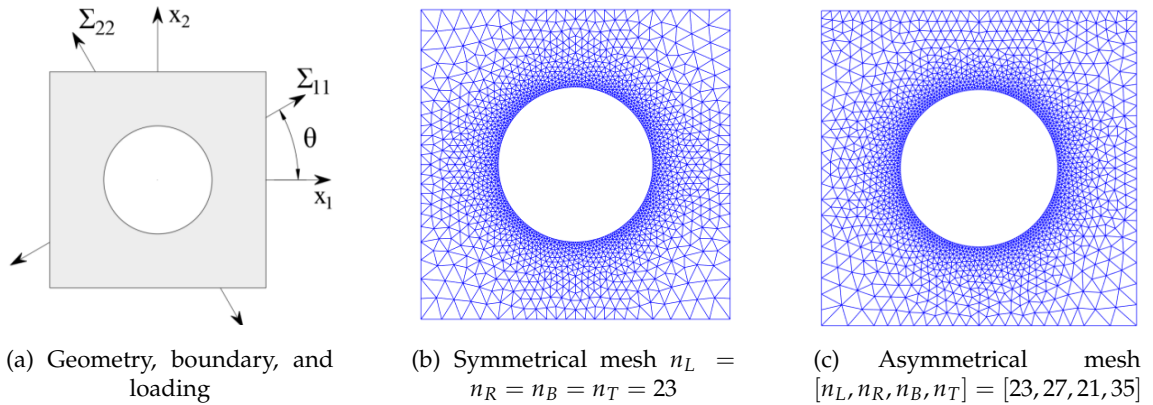
Fig. 3. RVE with a circular perforate at the center

into 20 segments, resulting in a 20$^{\text{th}}$-order polynomial for the Lagrange interpolation. In contrast, a piecewise cubic Hermite polynomial associated with each sub-interval is generated for the spline interpolation scheme.

Table 1. Circular perforated RVE: uniaxial strength (Σ_{11}/σ_p) with different periodic boundary enforcement strategies

Approach	N_e	N_{var}	λ^+	
			$\theta = 0°$	$\theta = 45°$
Standard periodic boundary	5960	30195	0.5586	0.4806
Lagrange interpolation boundary	5916	30127	0.5622	0.4823
Cubic spline interpolation boundary	5916	30287	0.5589	0.4812

Table 1 shows the comparison of solutions obtained using the three models above. The results from the Lagrange and cubic spline interpolating formulations-based methods are in good agreement compared to those given by the standard periodic boundary-based procedure. The similarity of the boundary periodicity can also be seen in Fig. 4, where the displacement fields are plotted. In terms of accuracy, the comparison in Table 1 indicates that when using a similar mesh and additive periodic points, the overall efficient strengths achieved by cubic Hermite spline interpolation are slightly better than those by the Lagrange interpolation technique.

Fig. 5 shows the distributions of dissipation power and the comparison of solutions with other studies for various cases of inclination angle and perforated radius. It can be observed that for all loading inclinations, the limit load factors decrease when the perforate size increases. The comparison in Fig. 5(c) demonstrates the excellent agreement between the present solutions and others in the literature.

Standard periodic boundary
(symmetrical mesh)

Lagrange interpolation
(asymmetrical mesh)

Cubic spline interpolation
(asymmetrical mesh)

(a) $\theta = 0°$

(b) $\theta = 45°$
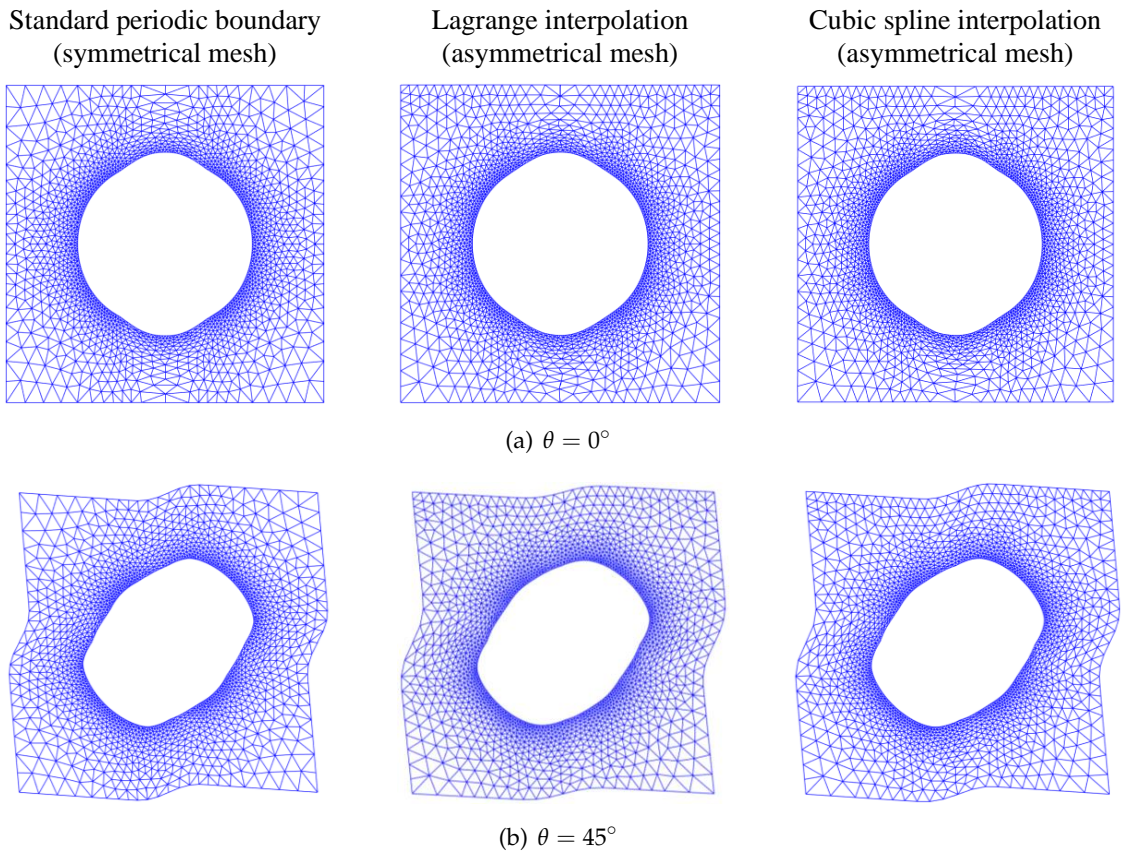
Fig. 4. Circular perforated RVE: displacement fields with three different periodic boundary
enforcement strategies

(a) $\theta = 0°$

(b) $\theta = 45°$

(c) The comparison of solutions
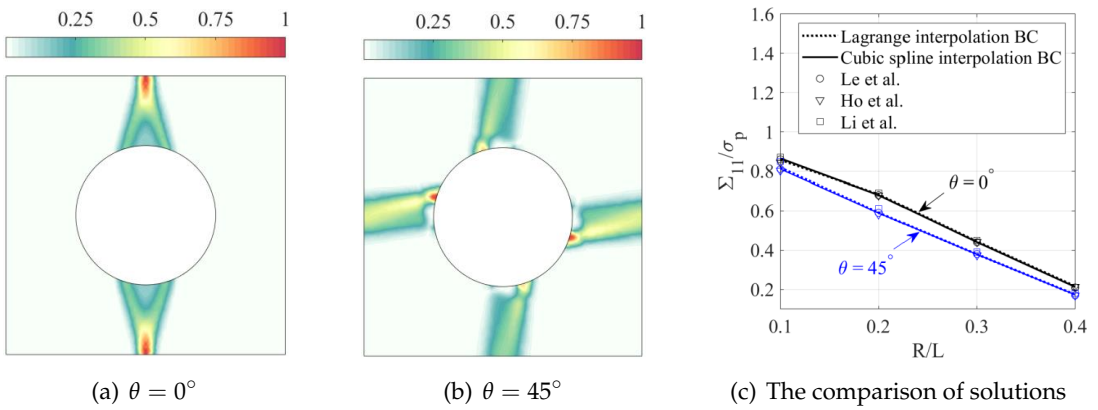
Fig. 5. Circular perforated RVE: collapse mechanisms and comparison with other studies

5.2. RVE with the irregular distributions of holes

In this example, an RVE containing randomly distributed porous material is examined. The space occupied by the porous is described as equally sized circles such that their total volume accounts for 25% of the RVE volume. The problem is considered with 10, 50 and 100 holes, as shown in Fig. 6, and the loading inclination $\theta = 0°$.

|(a) 10 holes|(b) 50 holes|(c) 100 holes|

Fig. 6. RVE with arbitrary distributions of holes

10 holes   50 holes   100 holes

$\lambda^+ = 0.3627$ $\lambda^+ = 0.3173$ $\lambda^+ = 0.3578$

(a) Lagrange interpolation

$\lambda^+ = 0.3604$ $\lambda^+ = 0.3165$ $\lambda^+ = 0.3551$

(b) Cubic spline interpolation
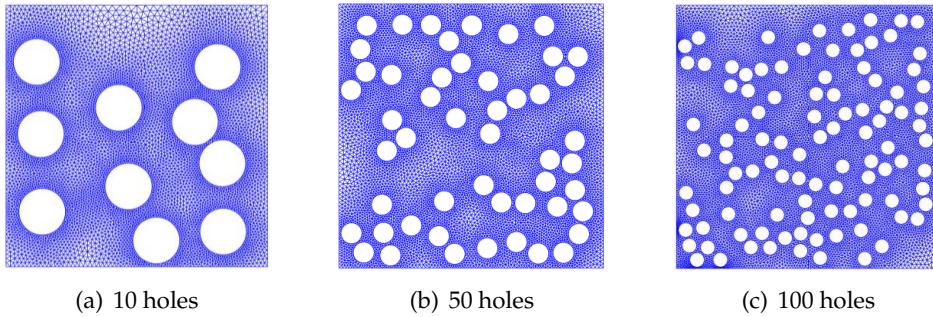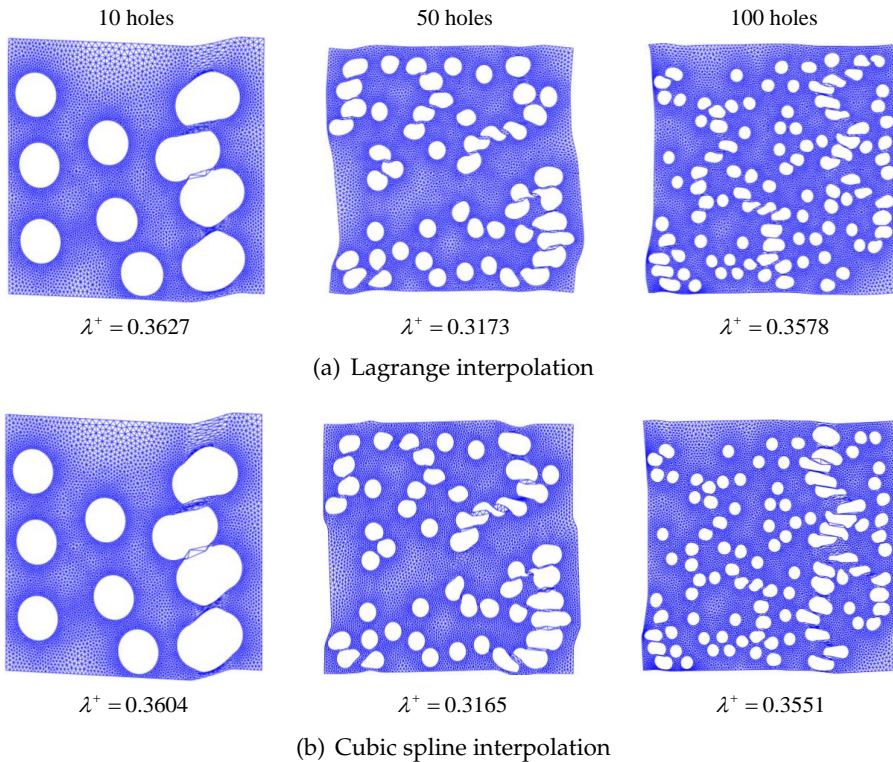
Fig. 7. RVE with arbitrary distributions of holes: displacement fields and macroscopic strengths

Fig. 7 shows the displacement fields and the limit load multipliers obtained using Lagrange and cubic spline interpolating formulations. It can be observed that both methods of imposing periodic boundary conditions give very similar results. The cubic spline interpolation scheme provides better (lower) solutions, whereas the Lagrange interpolation results in smoother displacement fields. The collapse mechanisms for various hole distributions are also captured in Fig. 8.
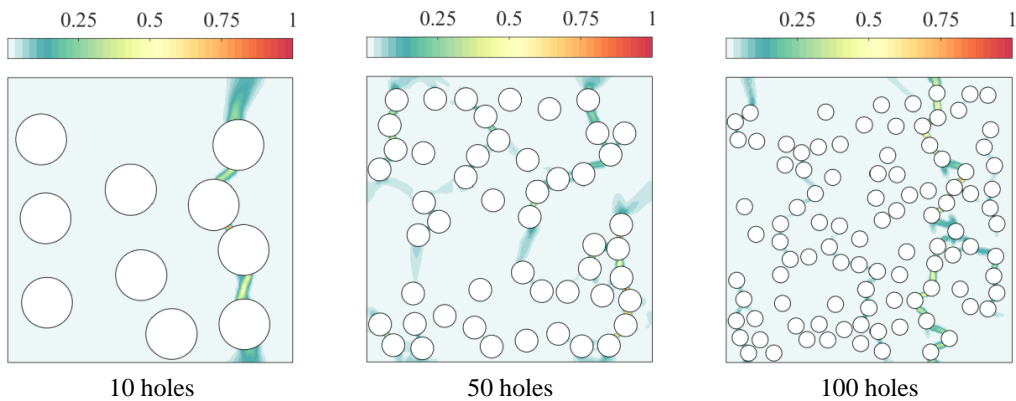
Fig. 8. RVE with arbitrary distributions of holes: distributions of dissipation power

6. CONCLUSIONS

This study has developed the treatments for imposing the periodic boundary condition of the asymmetrical RVE in the yield design computational homogenization framework. Two interpolating strategies are suggested based on the Lagrange polynomial and cubic spline polynomial. The periodic conditions are indirectly enforced by interpolating the fluctuating displacements of boundary nodes passing through a set of additive artificial points, periodic in pairs on RVE boundary. By casting the optimization problems as second-order cone programming, the number of variables and constraints is kept at a minimum. The numerical examples demonstrate computational efficiency of the proposed method. The crucial information for yield design, such as ultimate macroscopic strengths and collapse mechanisms, is also provided.

DECLARATION OF COMPETING INTEREST

The authors declare that they have no known competing financial interests or personal relationships that could have appeared to influence the work reported in this paper.

FUNDING

REFERENCES

[1] J. C. Michel, H. Moulinec, and P. Suquet. Effective properties of composite materials with periodic microstructure: a computational approach. *Computer Methods in Applied Mechanics and Engineering*, **172**, (1999), pp. 109–143. https://doi.org/10.1016/s0045-7825(98)00227-8.

[2] V. Kouznetsova, W. A. M. Brekelmans, and F. P. T. Baaijens. An approach to micro-macro modeling of heterogeneous materials. *Computational Mechanics*, **27**, (2001), pp. 37–48. https://doi.org/10.1007/s004660000212.

[3] C. Miehe and A. Koch. Computational micro-to-macro transitions of discretized microstructures undergoing small strains. *Archive of Applied Mechanics (Ingenieur Archiv)*, **72**, (2002), pp. 300–317. https://doi.org/10.1007/s00419-002-0212-2.

[4] M. G. D. Geers, V. G. Kouznetsova, and W. A. M. Brekelmans. Multi-scale computational homogenization: Trends and challenges. *Journal of Computational and Applied Mathematics*, **234**, (2010), pp. 2175–2182. https://doi.org/10.1016/j.cam.2009.08.077.

[5] K. Terada, M. Hori, T. Kyoya, and N. Kikuchi. Simulation of the multi-scale convergence in computational homogenization approaches. *International Journal of Solids and Structures*, **37**, (2000), pp. 2285–2311. https://doi.org/10.1016/s0020-7683(98)00341-2.

[6] F. Larsson, K. Runesson, S. Saroukhani, and R. Vafadari. Computational homogenization based on a weak format of micro-periodicity for RVE-problems. *Computer Methods in Applied Mechanics and Engineering*, **200**, (2011), pp. 11–26. https://doi.org/10.1016/j.cma.2010.06.023.

[7] J. M. Tyrus, M. Gosz, and E. DeSantiago. A local finite element implementation for imposing periodic boundary conditions on composite micromechanical models. *International Journal of Solids and Structures*, **44**, (2007), pp. 2972–2989. https://doi.org/10.1016/j.ijsolstr.2006.08.040.

[8] Z. Yuan and J. Fish. Toward realization of computational homogenization in practice. *International Journal for Numerical Methods in Engineering*, **73**, (3), (2007), pp. 361–380. https://doi.org/10.1002/nme.2074.

[9] V.-D. Nguyen, E. Béchet, C. Geuzaine, and L. Noels. Imposing periodic boundary condition on arbitrary meshes by polynomial interpolation. *Computational Materials Science*, **55**, (2012), pp. 390–406. https://doi.org/10.1016/j.commatsci.2011.10.017.

[10] R. Wang, L. Zhang, D. Hu, C. Liu, X. Shen, C. Cho, and B. Li. A novel approach to impose periodic boundary condition on braided composite RVE model based on RPIM. *Composite Structures*, **163**, (2017), pp. 77–88. https://doi.org/10.1016/j.compstruct.2016.12.032.

[11] V. Carvelli, G. Maier, and A. Taliercio. Kinematic limit analysis of periodic heterogeneous media. *CMES (Computer Modelling in Engineering & Sciences)*, **1**, (2), (2000), pp. 19–30.

[12] H. Li, Y. Liu, X. Feng, and Z. Cen. Limit analysis of ductile composites based on homogenization theory. *Proceedings of the Royal Society of London. Series A: Mathematical, Physical and Engineering Sciences*, **459**, (2003), pp. 659–675. https://doi.org/10.1098/rspa.2002.1039.

[13] C. V. Le, P. H. Nguyen, H. Askes, and D. C. Pham. A computational homogenization approach for limit analysis of heterogeneous materials. *International Journal for Numerical Methods in Engineering*, **112**, (2017), pp. 1381–1401. https://doi.org/10.1002/nme.5561.

[14] P. L. H. Ho, C. V. Le, and P. H. Nguyen. Kinematic yield design computational homogenization of micro-structures using the stabilized iRBF mesh-free method. *Applied Mathematical Modelling*, **91**, (2021), pp. 322–334. https://doi.org/10.1016/j.apm.2020.09.056.